A new criterion for determining the representative elementary volume of translucent porous media and inner contaminant

Ming Wu[1, 2], Jianfeng Wu[2*], Jichun Wu[2], and Bill X. Hu[1*]

[1] Institute of Groundwater and Earth Sciences, Jinan University, Guangzhou 510632, China

[2] Key Laboratory of Surficial Geochemistry, Ministry of Education; Department of Hydrosciences, School of Earth Sciences and Engineering, Nanjing University, Nanjing 210023, China

Correspondence to: J.F. Wu (jfwu@nju.edu.cn), B.X. Hu (billhu@jnu.edu.cn)

ABSTRACT

Representative elementary volume (REV) is essential to measure and quantify the effective parameters of a complex heterogeneous medium. To overcome the limitations of the existing REV estimation criteria, a new REV estimation criterion (χ^i) based on dimensionless range and gradient calculation is proposed in this study to estimate REV of a translucent material based on light transmission techniques. Three sandbox experiments are performed to estimate REVs of porosity, density, tortuosity and perchloroethylene (PCE) plume using multiple REV estimation criteria. In comparison with χ^i, previous REV estimation criteria based on the coefficient of variation (C_V^i), the entropy dimension (DI^i) and the relative gradient error (ε_g^i) are tested in REV quantification of translucent silica and inner PCE plume to achieve their corresponding effects. Results suggest that new criterion (χ^i) can effectively identify the REV in the materials, whereas the coefficient of variation and entropy dimension (DI^i)are not effective. The relative gradient error can make the REV plateau obvious, while random fluctuations make the REV plateau uneasy to identify accurately. Therefore, the new criterion is appropriate for REV estimation of the translucent materials and inner contaminant. Models are built based on Gaussian equation to simulate the distribution of REVs for media properties, which frequency of REV is dense in the middle and sparse on both sides. REV estimation of PCE plume indicates high level of porosity lead to large value of mean and standard deviation for REVs of PCE saturation (S_o) and PCE-water interfacial area (A_{OW}). Fitted equations are derived from distribution of REVs for PCE plume related to d_m (distances from mass center to considered point) and d_I (distances from injection position to considered point). Moreover, relationships between

REVs of PCE plume and S_o are fitted using regression analysis. Results suggest a decreasing trend appears for S_o-REV when S_o increases, while A_{ow}-REV increases with increasing of S_o.

Keywords: new criterion; representative elementary volume (REV); translucent material

1. Introduction

Modelling groundwater and contaminant (such as hazardous irons) transport in subsurface environment is based on the premise that micro-structure of aquifer exist a representative elementary volume (REV) (Wang et al., 2016; Lei and Shi, 2019). REV acts as a micro-scale characteristic, which is important to improve our understanding of materials, inner fluid flow and other processes (Brown and Hsieh, 2000; Costanza-Robinson et al., 2011; Wu et al., 2017). Previous studies suggested that even the Platinum-Nanoparticle-Catalyzed hydrogenation reactions and ion transport through angstrom-scale slits in cell activity existed apparent size effect, implying size effect is a wide characteristic for many process and materials (Bai et al., 2016; Esfandiar et al., 2017). With the help of REV, a porous medium can be treated as continuum medium (Brown and Hsieh, 2000; Kang et al., 2003; Müller and Siegesmund, 2010; Teruel and Rizwan-uddin, 2010; Hendrick et al., 2012; Wang et al., 2012; Ukrainczyk and Koenders, 2014; Kim and Mohanty, 2016; Gilevska et al., 2019). A conceptual representation of "REV curve" (Brown and Hsieh, 2000), characterizing porosity (θ) change with measured scale (L) increment, is presented in Fig. 1a. Based on the characteristic of REV curve in Fig. 1a, the REV curve can be divided into three regions. When measured scale (Fig. 1b) is in region I, the porosity fluctuates drastically at small scales. As measured scale size ranging between L_{min} and L_{max}, a flat

plateau with constant and steady value is encountered and the property is factored into its average value. Material property in spatial scales less than L_{min} is spatially varied portions with small scale, which can be easily influenced by individual pores in micro-structure such as region I (Fig. 1a). Likewise, material property is allowed drift to new values in spatial scale above L_{max} due to additional morphological structures of large field heterogeneity (region III). As a matter of fact, REV scale of region II can be derived between the small and spatially varied property in region I and large field variability in region III. However, the lower and upper boundaries L_{min} and L_{max} of REV plateau is hard to be identified in reality (Brown and Hsieh, 2000; Costanza-Robinson et al., 2011).

As technology advanced and progressed, non-destructive and non-invasive techniques of x-ray and gamma ray micro-tomography were utilized for micro-structure characteristic measurement in materials (Ghilardi, 1993; Brown and Hsieh, 2000; Niemet and Selker, 2001; Bob et al., 2008; Al-Raoush and Papadopoulos, 2010; Costanza-Robinson et al., 2011; Al-Raoush, 2012; Borges and Pires, 2012; Fernandes et al., 2012; Rozenbaum and Roscoat, 2014; Pereira Nunes et al., 2016; Piccoli et al., 2019). Generally, REV estimation for material properties, inner gas and fluid also was usually implemented by micro visualization and scanning of X-ray and gamma ray in laboratory (Brown and Hsieh, 2000; Razavi et al., 2007; Nordahl and Ringrose, 2008; Al-Raoush and Papadopoulos, 2010; Costanza-Robinson et al., 2011; Rozenbaum and Roscoat, 2014; Borges et al., 2018), while different criteria were utilized to quantify REV (Brown and Hsieh, 2000; Martínez et al., 2007; Nordahl and Ringrose, 2008; Costanza-Robinson et al., 2011). Lower boundary scale L_{min} of REV was identified by means of entropy dimension (DI^i) for eight soil samples (Martínez

et al., 2007). Further, REV scale of permeability for ripple laminated sandstone intercalated with mudstone was estimated using the coefficient of variation (C_V^i), which the REV scale is identified by the variability among the ten samples to achieve average REV scale (Nordahl and Ringrose, 2008). As a result, only one REV boundary was identified and not every sample can be estimated effectively (Nordahl and Ringrose, 2008). More interestingly, REV of material property (porosity), moisture saturation and air-water interfacial areas in porous media were estimated by a criterion named the relative gradient error (ε_g^i)(Costanza-Robinson et al., 2011). REVs of permeability of translucent material, PCE saturation and PCE-water interfacial area also can be estimated using the relative gradient error (Wu et al., 2017). In summary, the REV estimation was made by multiple kinds of criteria, while the REV identification effects of these criteria were not clear. What's more, these previous criteria estimate REV scale unsatisfactorily that beginning and ending of REV plateau can't be identified simultaneously for translucent porous media based on light transmission technique. Therefore, new criterion which can identify REV plateau accurately is needed.

In this study, a new criterion (χ^i) for REV estimation is proposed to identify the REV scale of the translucent silica and inner contaminant. Three perchloroethylene (PCE) transport experiments are conducted in two dimensional (2D) sandboxes to test the effect of different REV estimation criteria. Translucent silica is selected for associated REV analysis due to its extensive utilization in laboratory experiment of exploring groundwater flow and contaminant migration behavior in micro-structure of a sandy aquifer (Niemet and Selker, 2001; Bob et al., 2008; Costanza-Robinson et al., 2011). Moreover, translucent silica is also

an important material applied in numerous industries (Bouvry et al., 2016). In laboratory experiments, translucent silica is packed in 2D sandboxes where porosity, density, tortuosity and PCE saturation are derived by light transmission technique (Fig. 1c). Porosity and PCE saturation are selected as the representative variables to explore corresponding REV estimation by different criteria, which is very essential and significant for REV identification. Previous criteria such as the coefficient of variation (C_V^i), entropy dimension (DI^i), the relative gradient error (ε_g^i) and the new criterion-χ^i are tested in REV estimation. Associated effects are analyzed to achieve the best criterion of effective and appropriate quantification of REV.

2. Experiment procedure and method

2.1 Experiment

Three sandboxes (Fig. 2a-c) packed by translucent silica medium are prepared in laboratory to test different criteria of REV quantification. PCE is selected as a typical DNAPL contaminant used in experiments. 2D sandbox is composed by three aluminum interior frames and two glass walls, which thickness is 1.6cm. The dimensions of sandboxes used in Experiment-I are 20 (width) ×15 (height), and the dimensions of Experiments-II and III are 60 (width)×45 (height). F40/50 and F20/30 mesh translucent silica sands are used for background material for Experiments-I and II, while heterogeneous translucent silica with low porosity and permeability are packed in sandbox for Experiment-III. To make the translucent silica fully saturated by water in a flow field close to natural groundwater environment (Erning et al., 2012), water flow at flow velocity of 0.5 m/d is set from left to right in laboratory sandbox experiments (Fig. 2a-c). Water is restricted in a sandbox that the

top and bottom layers of the sandbox are packed by F70/80 mesh translucent silica as capillary barriers. Light source is placed behind the sandbox to make light penetrate through translucent media and capture emergent light intensity using a thermoelectrically air-cooled charge-coupled device (CCD) camera (Fig. 1c). Afterward, PCE is injected into sandboxes from the injection needle at constant rate of 0.5 mL /min for three experiments. Detailed experimental conditions are listed in Table 1.

2.2 Light transmission technique

By means of light transmission technique (Fig. 1c), DNAPL and water saturation can be obtained rapidly and in real-time, which greatly help to explore the mechanism of groundwater flow and contaminant migration in porous media. When light passes through translucent materials of a given thickness, the emergent light intensity after the absorptive and interfacial losses can be expressed as (Niemet and Selker, 2001; Bob et al., 2008; Wu et al., 2017):

$$I_T = CI_0(\prod \tau_b)\exp(-\sum \alpha_a d_a) \quad (1)$$

where a represents phase number; b represent the number of the interface between phase a and a+1; I_0 is the original light intensity; C is a constant of correction for light emission and light observation; τ_b is the transmittance when light penetrate from phase a to a+1; α_a is the absorption coefficient when light penetrate in phase a; d_a is the length of light penetration path in phase a.

To derive the porosity, the 2D translucent porous medium should be only saturated by water. Consequently, the emergent light intensity can be expressed as (Niemet and Selker, 2001; Bob et al., 2008; Wu et al., 2017):

$$I_s = CI_0 \tau_{s,w}^{2k_o} \exp(-\alpha_s k_s d_s) \quad (2)$$

where $\tau_{s,w}^{2k_0}$ is the transmittance of solid-water interface; α_s is solid particles absorption coefficient; d_s is median diameter of the solid particles; k_o is the number of pores across light penetration path; k_s is the number of solid particles across light penetration path.

If we arbitrarily select an infinitesimal element, its area A_o approaches zero ($A_o \rightarrow 0$) from the 2D translucent porous media (Fig. 1d), and suppose the infinitesimal element with thickness L_T containing solid particles and pores that can be regarded as lamellar structure (Fig. 1d), we can obtain the following relationships (Wu et al., 2017):

$$\theta A_o L_T = A_o k_o d_o \quad (3)$$

$$k_s d_s + k_o d_o = L_T \quad (4)$$

where d_o is the median diameter of pores; θ is porosity.

Substituting Eq. (3) and Eq. (4) into Eq. (2), the relationship between emergent light intensity and porosity can be achieved (Wu et al., 2017):

$$lnI_s = \beta + \theta\gamma \quad (5)$$

where $\beta = \ln(\frac{CI_s}{e^{\alpha_s d_s L_T}})$ and $\gamma = \ln(\tau_{s,w}^{\frac{2L_T}{d_0}} e^{\alpha_s L_T})$. β and γ can be determined from experimental data, then porosity can be obtained.

The density and tortuosity are derived as (Wu et al., 2018):

$$\rho = \theta\rho_w + (1.0 - \theta)\rho_s \quad (6)$$

$$\tau = 1 + \frac{\pi - 2}{\sqrt{\frac{\pi}{1-\theta}}} \quad (7)$$

where ρ is the density of translucent porous media; ρ_w is the density of water; ρ_s is the density of solid particles; τ is tortuosity.

165 The saturation of dense nonaqueous phase liquid (DNAPL) was quantified by light
166 transmission technique based on light pass through translucent materials (Niemet and Selker,
167 2001; Bob et al., 2008):

168 $$S_o = \frac{\ln I_s - \ln I_T}{\ln I_s - \ln I_{oil}} \quad (8)$$

169 where S_o is the saturation of DNAPL; I_s is the light intensity after light penetration through
170 translucent porous when all pores are fully saturated by water; I_{oil} is the light intensity
171 when all pores are fully saturated by DNAPL; I_T is the light intensity after penetration
172 through translucent materials. After quantification of PCE saturation, PCE-water interfacial
173 area (A_{OW}) can be obtained based on the method proposed by Wu et al. (2017), where the
174 unit of A_{OW} is cm^{-1}.

175 Emergent light intensity for three experiments is captured by a thermoelectrically air-
176 cooled charge-coupled device (CCD) camera (Niemet and Selker, 2001; Bob et al., 2008).
177 Every pixel with small scale could be approximated as infinitesimal element in high
178 resolution image to apply light transmission techniques. As consequence, porosity of
179 translucent silica was derived using light transmission technique through Eq. (5). The whole
180 2D translucent silica area was numerically discretized that every cell had the uniform
181 dimensions of 0.015m×0.015m. The cuboid window (Fig. 1b) was utilized to quantify the
182 variables (porosity, density, tortuosity, PCE saturation, PCE-water interfacial area) of every
183 cell as measured scale was increased. In detail, the measured cuboid window scale was
184 increased from the center of each cell and associated value of variable was calculated from
185 the high resolution porosity of 2D translucent silica derived by light transmission technique.
186 Observation cells were selected from the discretized cells (Fig. 3b) of which the cells I-1~2,

187 II-1~2 and III-1~2 belong to Experiments-I-III, respectively.

188 To analyze the regularity of REV distribution for PCE plume, the mass center
189 coordinate and the granglia-to-pool ratio (GTP) of PCE plume are quantified for
190 Experiments-I-III. The mass center coordinate and GTP are calculated as:

191 $$X_m = \frac{M_{10}}{M_{00}} \tag{9}$$

192 $$Z_m = \frac{M_{01}}{M_{00}} \tag{10}$$

193 $$GTP = \frac{V_{ganglia}}{V_{pool}} \tag{11}$$

194 where X_m is x coordinate of mass center for PCE plume; Z_m is z coordinate of mass center
195 for PCE plume; GTP is granglia-to-pool ratio, which equals to the ratio of the $V_{ganglia}$ to
196 V_{pool}; $V_{ganglia}$ is the PCE volume under ganglia state; V_{pool} is the PCE volume under pool
197 state; M_{00}, M_{10} and M_{01} are computed using definition of spatial moment (M_{ij}),
198 $M_{ij} = \int_{x_0}^{x_1}\int_{z_0}^{z_1}\theta(x,z)S_o(x,z,t)x^i z^j d_x d_z$; x_0 and z_0 are minimum limits of x axis and z axis; x_1
199 and z_1 are maximum limits of x axis and z axis; θ(x,z) is the porosity at point (x,z); S_o(x,z,t)
200 is PCE saturation of point (x, z) at time t.

201 2.3 Criteria of REV quantification

202 The REV is defined as the volume range in which all material characteristics are
203 factored into the average and associated values approach single and constant (Brown
204 and Hsieh, 2000). In the range of REV, the value of one associated property will meet
205 the condition:

206 $$\frac{\partial Y(L_i)}{\partial L}\Big|_{L_i=L_o} = 0 \tag{12}$$

207 where the $Y(L_i)$ is the value of an associated property when system scale is L_i; L_i is the

value of system scale; L_o is the scale range of REV, $L_{min}<L_o<L_{max}$; L_{max} is upper boundary of REV; L_{min} is lower boundary of REV scale. According to the Eq. (12), when the measured scale (L_i) reaches REV range, $\frac{\partial Y(L_i)}{\partial L} \to 0$. As a matter of fact, most previously used criteria were applied to estimate REV based on this requirement (Brown and Hsieh, 2000; Martínez et al., 2007; Nordahl and Ringrose, 2008; Costanza-Robinson et al., 2011).

To evaluate the REV of porosity, the coefficient of variation (C_V^i) is utilized to estimate the variability (Nordahl and Ringrose, 2008):

$$C_V^i = \frac{\hat{s}_i}{\overline{\varphi}_i} \tag{13}$$

where i is the cuboid window (Fig. 1b) increment number; φ is the measured variable, such as porosity; $\hat{s}_i$ is the standard deviation of sub-grids' variable in different measured volume or scale; $\overline{\varphi}_i$ is the arithmetic average of the variable values in the sub-grids. When number of sub-grids (N) is less than 10, a correction is utilized to replace Eq. (13). According to Nordahl and Ringrose (2008), $0 < C_V^i < 0.5$ is defined as homogeneous and $C_V^i = 0.5$ can be used as criterion to identify the REV scale.

Similarly, for porosity of translucent silica, entropy dimension (DI^i) is utilized for REV analysis and estimation (Martínez et al., 2007), which is defined as:

$$DI^i \approx \frac{\sum_{j=1}^{m(i)} \mu_j(L_\varepsilon) \log \mu_j(L_\varepsilon)}{\log L_\varepsilon} \tag{14}$$

where, L_ε is the scale of sub-grid; "≈" indicates the asymptotic equivalence as $L_\varepsilon \to 0$ (Martínez et al., 2007); j is the ordinal number of sub-grid in measured cuboid window (Fig. 1b) of increment number i; $m(i)$ is the total number of sub-grids in measured cuboid window (Fig. 1b) of increment number i; $\mu_j(\varepsilon)$ is the proportion of the variable of sub-

grid j in the whole measured cuboid window i. The right hand side of Eq. (14) is the simplification of Shannon entropy of all sub-grids, in which DI^i can be considered as the average of logarithmic values of the variable distribution weighted by $\mu_j(L_\varepsilon)$ to quantify the degree of medium heterogeneity. Using Eq. (14), a series of values of DI^i (i=1,2,3…) are obtained for each measured cuboid window (Fig. 1b) of increment number i. For estimation of the REV in a porous medium, the relative increment of entropy dimension and associated criterion of REV identification are respectively expressed as:

$$RI^i = |\frac{DI^j - DI^{j-1}}{DI^{j-1}}| \times 100 \quad (15)$$

$$RI^i \leqslant 0.2CV_{DI} \quad (16)$$

where CV_{DI} is the coefficient of variation of DI^i series (i=1,2,3…), which is calculated through $CV_{DI} = (\hat{s}_{DI}/\overline{DI}) \times 100$; $\overline{DI}$ is the mean value of the DI^i series; $\hat{s}_{DI}$ is the standard deviation of the DI^i series.

To achieve the REV for multiple system variables, such as porosity, moisture saturation and air-water interfacial areas in an unsaturated porous medium, a criterion named the relative gradient error was applied (Costanza-Robinson et al., 2011):

$$\varepsilon_g^i = |\frac{\varphi^{i+1} - \varphi^{i-1}}{\varphi^{i+1} + \varphi^{i-1}}| \frac{1}{\Delta L} \quad (17)$$

where ε_g^i is relative gradient error; ΔL is the measured cuboid window size increment length for REV estimation. Usually, ε_g^i less than 0.2 (Costanza-Robinson et al., 2011) is utilized to identify a REV sizes.

According to the requirement in Eq. (12), a new criterion based on the required condition of REV is proposed to estimate the REV range of the translucent silica in this study:

$$\chi^i = \frac{|\delta^{i+1} - \delta^{i-1}|}{\delta^i \Delta L} \quad (18)$$

where δ^i is the dimensionless range, $\delta^i = \frac{\varphi(L_i)_{max} - \varphi(L_i)_{min}}{\overline{\varphi(L_i)}}$; $\varphi(L_i)_{max}$ is the maximum value of the variable on the volume scale L_i; $\varphi(L_i)_{min}$ is the minimum value of the variable on the volume scale L_i; $\overline{\varphi(L_i)}$ is the mean value of the variable on the volume scale L_i. Brown and Hsieh (2000) suggested $\delta^i = \frac{\varphi(L_i)_{max} - \varphi(L_i)_{min}}{\overline{\varphi(L_i)}} << 1$ can be used for REV estimation. In fact, the calculated value of δ^i mostly is less than 1, while $\delta^i << 1$ is hard to be used to identify the REV scale for realistic materials, such as the translucent silica used in this study. The value limit of χ^i used for REV estimation also is explored in this study.

In this study, criteria for the coefficient of variation (C_V^i), entropy dimension (DI^i), the relative gradient error (ε_g^i) and the new criterion (χ^i) are all applied to REV estimation for porosity and PCE saturation. Corresponding REV plateau identification effects are compared to select the best criterion for REV quantification.

3. Results and discussion

3.1 REV identification effect of different criteria

3.1.1 The coefficient of variation

Emergent light intensity distributions of translucent silica for three experiments, which had been fully saturated by water, were obtained by a thermoelectrically air-cooled CCD camera (Niemet and Selker, 2001; Bob et al., 2008). The porosity, density, tortuosity and PCE saturation for three experiments are derived by light transmission technique as shown in Figs. 3a and b. The PCE spreads from the injecting point shaped like a drop of water at t=5 min (Fig. 3b). In 2D sandboxes for three experiments, PCE plume infiltrates in

274 translucent silica sands and reaches the bottom after t=80 min.

275 Porosity and PCE saturation variation curves of all observation cells with increasing
276 measured cuboid window scale were shown in Figs. 4a and b. However, for all observation
277 cells from translucent silica, the REV plateaus were not obvious to be objectively judged
278 visually, which made REV plateaus hard to identify effectively by original variation curves
279 for porosity and PCE saturation (Figs. 4a and b).

280 To make the REV plateau more explicit, different criteria of REV quantification are
281 utilized. The coefficient of variation (C_V^i) of porosity and PCE saturation fluctuating with
282 increasing of measured cuboid window size is shown in Fig. 4. The measured cuboid
283 window scale is limited to the dimensions of cells in discretization of 2D translucent
284 silica. The observation cells show various characteristics of variation tendency for the
285 coefficient of variation (C_V^i). The θ and S_o variation curves of the coefficient of variation
286 (C_V^i) for all observation cells do not reach stable values as those shown in Figs. 4a and b,
287 the beginning of the REV flat plateau is not easy to identify, the coefficient of variation (C_V^i)
288 is not suitable for REV estimation. According to the heterogeneity definition by Corbett and
289 Jensen (1992), the heterogeneity of materials is defined by C_V^i magnitude that $0 <$
290 $C_V^i < 0.5$ is classed as homogeneous medium, $0.5 < C_V^i < 1.0$ is classed as
291 heterogeneous medium and $1.0 < C_V^i$ is classed as strong heterogeneous medium. For
292 the coefficient of variation (C_V^i) magnitude in Figs. 4a and b, the C_V^i values are all below
293 0.5 that the criterion $C_V^i = 0.5$ is unable to identify the REV scale for translucent silica.

294 *3.1.2 Entropy dimension*

295 Entropy dimension (DI^i) is utilized by Martínez et al. (2007) for multifractal analysis
296 of a porous medium porosity and REV estimation. In this study, entropy dimension (DI^i) is
297 tested to avoid unclear REV plateau in porosity curves. The entropy dimension (DI^i) of
298 porosity is calculated by Eq. (14). Variation curves of entropy dimension (DI^i) for all
299 observation cells (Fig. 2a) are presented in Fig. 4. The curves of entropy dimension (DI^i) of
300 porosity and PCE saturation generally result in the increasing trend curves which makes
301 REV estimates become very difficult and invalid. Entropy dimension (DI^i) was quickly
302 increased with increasing of measured cuboid window size. Compared to the coefficient of
303 variation (C_V^i) of porosity and PCE saturation, entropy dimension (DI^i) increased step by
304 step without opposite fluctuation tendency in the variation curves as the length scale of
305 measured cuboid window increased simultaneously. In general, REV plateau in region II
306 (Fig. 1a) of porosity is not obvious for the entropy dimension (DI^i) curves of all observation
307 cells from three experiments, which suggests REV scales is uneasy to identify for
308 translucent silica using entropy dimension (DI^i) by light transmission technique.

309 *3.1.3 The relative gradient error*

310 The relative gradient error (ε_g^i) of porosity and PCE saturation is calculated by Eq.
311 (17). The variation of ε_g^i at different measured cuboid window scales is shown in Fig. 4
312 for all observation cells in the 2D translucent silica. For all ε_g^i curves at observation
313 cells from experiments, the REV plateaus in region II (Fig. 1a) are more clear than the
314 variation curves based on the criteria of C_V^i and DI^i. Apparently, erratic variations of

315 the relative gradient error (ε_g^i) at small measured cuboid window scales are observed for
316 all ε_g^i curves as the characteristic of REV region I in Fig. 1a. When measured cuboid
317 window scale further increases for all observation cells, the variability and magnitude of
318 the relative gradient error (ε_g^i) decrease well and factor into average, which can be
319 identified as REV plateau in region II (Fig. 1a). The relative gradient error (ε_g^i) makes the
320 REV plateau quantification convenient for all observation cells. At the measured cuboid
321 window size above the REV plateau, ε_g^i curves result in large variability for observation
322 cells I-1~2. These findings suggest that that the relative gradient error (ε_g^i) can make the
323 REV plateau more obvious, which greatly contribute to convenient and applicable REV
324 quantification for translucent silica by light transmission technique. However, random
325 fluctuations exist in ε_g^i curves visually, which make the REV plateau uneasy to identify
326 accurately.

327 *3.1.4 The new criterion (χ^i)*

328 χ^i of porosity and PCE saturation changing with measured cuboid window size is
329 shown in Fig. 4. Like the region I (Fig. 1a), erratic and random fluctuations appear at
330 small measured cuboid window sizes and χ^i increases with the increase of the measured
331 cuboid window size. When measured scale increases, the values of χ^i for all observation
332 cells appear fast reduction and rapidly tend to steady, which exhibit the characteristic of
333 REV plateau as measured scale reaches region II. The χ^i for observation cells restores the
334 erratic variation state of increasing trend after measured cuboid window size exceeding the
335 REV plateau. As shown in the variation curves of χ^i for all observation cells, the beginning
336 of the REV flat plateaus can be identified easily, suggesting χ^i is more convenient and

337 reliable than other methods for REV estimation. All observation cells show similar variation
338 curves of χ^i that low value intervals are quite apparent, indicating that χ^i is very effective to
339 make the REV plateau obvious for translucent silica used in this study. Using the criterion
340 of χ^i, the REV plateau of region II is flat, which is easily identified, compared with other
341 criteria for observation cells (Figs. 4a and b).

342 3.2 REVs of material properties

343 Based on the REV plateau identifications using the coefficient of variation
344 (C_V^i),entropy dimension (DI^i), the relative gradient error (ε_g^i) and the proposed new
345 criterion χ^i in Figs. 4a and b, the new criterion χ^i appears to be the most appropriate criterion
346 for REV plateau identification. Even though the relative gradient error (ε_g^i) can also make
347 REV plateau obvious, but various random fluctuations weaken the method and reduce the
348 associated accuracy. Therefore, REVs of porosity, density, tortuosity and PCE plume are
349 estimated using the new criterion χ^i in the following study.

350 In fact, large number of discretized cells in the 2D translucent silica for three
351 experiments are quantified using the new criterion χ^i, which is convenient to examine the
352 regularities for REV sizes and related factors. Using the new criterion χ^i, the REV estimation
353 is conducted based on Eq. (18). Fig. 5a shows minimum REV sizes of porosity, density and
354 tortuosity quantified by χ^i for all cells of three experiments. Associated statistical analysis
355 for REVs is illustrated in Fig. 5b, where circular points represent frequency and triangular
356 points represent cumulative frequency. Frequency of REVs is dense in the middle and sparse
357 on both sides, so the distribution of REVs can be fitted by Gaussian equation:

358 $$F = \omega + \frac{1}{\sqrt{2\pi}\epsilon} e^{-\frac{(REV-\nu)^2}{2\epsilon^2}} \quad (19)$$

where F is the frequency of REV; ω, ϵ and ν are fitted parameters of the model.

After regression analysis, the derived models for REV frequency are listed in Table 2. The coefficients of determination (R^2) of models for REVs of porosity and density for three experiments all exceed 0.85. R^2 for REV of tortuosity for three experiments exceeds 0.76. Moreover, the computed cumulative frequency based on models fit cumulative frequency from experimental results well in Fig. 5b.

The minimum REV size frequency of porosity appears a peak between 4.0 mm and 5.0 mm for Experiment-I. As minimum REV size of porosity increases, corresponding frequency continuously decreases. Further, smooth convex shape of cumulative frequency is observed for minimum REV size of porosity (Fig. 5b). Most minimum REV sizes of translucent silica distributed in 0.0-7.0mm. For density of translucent silica sand, associated REV frequency appears high values between 2.0~3.0 mm. For the REV sizes of tortuosity, minimum REV sizes distribute in 0.0~6.0 mm. Compared with Experiment-I (F40/50 mesh translucent silica sand), the frequency of REV for Experiment-II (F20/30 mesh translucent silica sand with larger porosity) shows flat shape and has larger value of standard deviation, especially for REV of porosity. Fig. 5b shows that translucent silica with larger porosity will achieve border distribution of minimum REV sizes distribution compared to translucent silica with relative lower porosity. Moreover, the frequency of REV of porosity and permeability for Experiment-III (background material is F20/30 mesh translucent silica sand with larger porosity, five lenses with lower porosity is packed in sandbox to create heterogeneity) is similar to the frequency of REV for Experiment-II. However, the frequency of τ-REV for Experiment-III is different from the frequency of τ-REV for

Experiment-II under homogeneous condition. The mean REV sizes of porosity, density and tortuosity for Experiment-I are 4.35 mm, 2.89 mm and 3.65 mm, respectively. All mean REV sizes of these variables for Experiment-II are larger than REVs of Experiments-I, which corresponding mean REV sizes are 8.05 mm, 2.97 mm and 4.30 mm. These results suggest translucent porous media with higher porosity lead to larger values of mean and standard deviation for REV sizes.

3.3 REVs of S_o and A_{OW} for PCE plume

Based on the new criterion χ^i and light transmission technique, the real-time distributions of S_o-REV and A_{OW}-REV for PCE plume can be obtained over the entire experimental period. The minimum REV sizes of S_o and A_{OW} obtained using new criterion χ^i are shown in Figs. 6a and b. When PCE migrates in sandbox, the REV of PCE plume is changed over time (Fig. 6). The REVs of PCE plume for Experiment-I mostly are lower than the REVs of PCE plume for Experiments-II and III. Moreover, when heterogeneous porous media is packed in sandbox, the REV distribution of Experiment-III become more heterogeneous compared with REV distribution of Experiments-II under homogeneous condition. Based on REV distributions of PCE plume for three experiments, statistical analysis is conducted to explore the regularity of REV distribution for PCE plume.

The mass center coordinate of PCE plume, GTP and plume area are shown in Fig. 7a. The values of X_m, Z_m and GTP for Experiment-II and III are higher than the X_m, Z_m and GTP of Experiment-I (lower porosity). Moreover, the plume area of Experiment-II is larger than the plume of Experiment-I. When packed material is heterogeneous, the plume area of PCE is increased further for Experiment-III. Besides, the mean and standard deviation of

REVs of PCE plume during 0~1523 min are derived by statistical analysis (Fig. 7a). Compared with REVs of PCE plume for Experiment-I, Experiment-II (F20/30 mesh translucent silica sand with higher porosity) has larger value of mean and standard deviation of REVs. The mean value of A_{OW}-REV for Experiment-III is much higher than A_{OW}-REV for Experiments-I and II.

The average value of REVs ($\overline{REV}$) and associated distance (d_m) from mass center to corresponding cells contained in PCE plume at t=1523 min are presented in Fig. 7b. Regression analysis is performed for average REVs of PCE plume and d_m, where fitted models and associated R^2 for Experiments-I-III are listed in Table 3. Simultaneously, the fitted equations between $\overline{REV}$ and d_I (the distance from injection point to cell contained in PCE plume) also are derived by regression analysis. From the results in Fig. 7a, $\overline{REV}$ of S_o and A_{ow} appear a peak and then decrease with increasing of d_m and d_I for Experiment-I. $\overline{REV}$ of S_o and A_{ow} for Experiment-I all firstly increase and then decrease with the increasing of d_m and d_I. However, $\overline{REV}$ of S_o presents apparent decreasing tendency as d_m and d_I increase for Experiment-II, and $\overline{REV}$ of A_{ow} just slightly increase first and then decrease for Experiment-II. In addition, the value of A_{OW}-REV mostly is higher than the value of S_o-REV for three experiments. Compared with the R^2 of the fitted relationship between average REVs of PCE plume and d_m, d_I for Experiments-I and II, the values of R^2 achieved by Experiment-III are much lower (Table 3).

Besides, the relationship between REVs and PCE saturation are fitted by regression analysis, where fitted equation and R^2 for three experiments are listed in Table 4 and Fig. 7b. With increasing of PCE saturation, REV of S_o appear decline trend for three experiments.

However, REV of A_{OW} increases when S_o increases for all three experiments (Fig. 7b). On the other hand, REV of S_o for Experiment-II is higher than corresponding REV for Experiment-I, while Experiments-I and II have similar values of A_{OW}-REV (Fig. 7b). Moreover, REVs of S_o and A_{OW} for Experiment-III are higher than REVs of S_o and A_{OW} for Experiments-I and II. These results suggest higher porosity will lead to high value of S_o-REV and the relationship between REVs of PCE plume and dm, d_l. S_o-REV and A_{OW}-REV are increased under heterogeneous condition.

4. Conclusions

In this study, a new criterion χ^i is proposed to identify the REVs of translucent porous media and inner contaminant transformation based on previous criteria. The REV plateaus of observation cells selected from three experiments of PCE transport are hard to judge visually from the porosity and PCE saturation curves. From the REV identification effects of different criteria, the REV flat plateau is difficult to identify by the coefficient of variation (C_V^i) and entropy dimension (DI^i), indicting the coefficient of variation (C_V^i) and entropy dimension (DI^i) are not suitable for REV estimation of translucent porous media. The relative gradient error (ε_g^i) can make REV plateaus of all kinds of translucent silica explicit in variation curves, but random fluctuations weaken REV plateau identification. In comparison with these previous criteria, the beginning and ending of the REV flat plateaus could be easily and directly identified in the curves based on the new criterion χ^i, suggesting the new criterion χ^i is more convenient and effective for REV estimation. In this study, REVs of porosity, density, tortuosity, and PCE plume are estimated using the new criterion χ^i.

Statistical results of minimum REV scales quantified by new criterion χ^i reveal

cumulative frequencies of porosity, density and tortuosity all have smooth convex shapes. Models based on Gaussian equation are built for the distribution of REVs of porosity, density and tortuosity, which porous media with larger porosity leads to larger values of mean and standard deviation for REV sizes of media properties. For REVs of PCE plume, result suggested larger porosity lead to larger value of mean and standard deviation. Regression analysis is performed to study the regularity for distribution of REVs, where fitted relationship between REVs and d_m, d_I are derived for PCE plume. $\overline{REV}$ of S_o and A_{ow} firstly increase and then decrease with the increasing of d_m and d_I for Experiment-I whose sandbox packed by translucent porous media with relatively lower porosity. However, $\overline{REV}$ of S_o and A_{ow} directly decrease with the increment of d_m and d_I when porosity became larger for Experiment-II. The values of R^2 of the fitted relationship between average REVs of PCE plume and d_m, d_I for Experiment-III are much lower under heterogeneous condition. Significantly, REV size of S_o presented decreasing trend as S_o increases, while increasing tendency appeared for REV size of A_{ow}. Through regression analysis, the fitted equations between REVs of PCE plume and PCE saturation are derived for three experiments. Implications of these finding are essential for quantitative investigation of scale effect of porous media and contaminant transformation. The fluid migration and transform in porous media can be simulated accurately according to the REV estimation results using light transmission technique and the appropriate criterion χ^i.

Code and data availability

The codes and data for this paper are available by contacting the corresponding author at

jfwu@nju.edu.cn.

Author contributions

Ming Wu: Conceptualization, Methodology, Writing;

Jianfeng Wu: Conceptualization, Methodology, Writing;

Jichun Wu: Conceptualization;

Bill X. Hu: Conceptualization, Writing.

Declaration of interests

The authors declare that they have no known competing financial interests or personal relationships that could have appeared to influence the work reported in this paper.

Acknowledgments

We acknowledge support by the National Key Research and Development Plan of China (2019YFC1805302 and 2016YFC0402800), the National Natural Science Foundation of China (41902246, 41730856 and 41772254), the Natural Science Foundation of Guangdong Province (2020A1515010447) and the Fundamental Research Funds for the Central Universities (14380105).

References

Al-Raoush, R., and Papadopoulos, A.: Representative elementary volume analysis of porous media using X-ray computed tomography, Power Technol., 200, 60-77, 2010.

Al-Raoush, R.: Change in Microstructure Parameters of Porous Media Over Representative

487 Elementary Volume for Porosity, Part. Sci. Technol., 30, 1-16, 2012.
488 Bai, L., Wang, X., Chen, Q., Ye, Y., Zheng, H., Guo, J., Yin, Y., and Gao, C.: Explaining the
489 Size Dependence in Platinum-Nanoparticle-Catalyzed Hydrogenation Reactions,
490 Angew. Chem. Int. Ed., 55, 15656-15661, 2016.
491 Bob, M.M., Brooks, M.C., Mravik, S.C., and Wood, A.L.: A modified light transmission
492 visualization method for DNAPL saturation measurements in 2-D models, Adv.
493 Water Resour., 31, 727-742, 2008.
494 Borges, J.A.R., and Pires, L.F.: Representative elementary area (REA) in soil bulk density
495 measurements through gamma ray computed tomography, Soil Till. Res., 123, 43-
496 49, 2012.
497 Borges, JAR., Pires, L.F., Cássaro, F.A.M., Roque, W.L., Heck, R.J., Rosa, J.A., and Wolf,
498 F.G.: X-ray microtomography analysis of representative elementary volume (REV)
499 of soil morphological and geometrical properties, Soil Till. Res., 182, 112-122,
500 2018.
501 Bouvry, B., del Campo, L., Meneses, D.D.S., Rozenbaum, O., Echegut, R., Lechevalier, D.,
502 Gaubil, M., and Echegut, P.: Hybrid methodology for retrieving thermal radiative
503 properties of semi-transparent ceramics, J. Phys. Chem. C, 120, 3267-3274, 2016.
504 Bradford, S.A., Vendlinski, R.A., and Abriola, L.M.: The entrapment and long-term
505 dissolution of tetrachloroethylene in fractional wettability porous media, Water
506 Resour. Res., 35(10), 295-2964, 1999.
507 Brown, G.O., and Hsieh, H.T.: Evaluation of laboratory dolomite core sample size using
508 representative elementary volume concepts, Water Resour. Res., 36(5), 1199-1207,

2000.

Corbett, P.W.M., and Jensen, J.L.: Estimating the mean permeability: how many measurement do we need? First Break, 10(3), 89-94, 1992.

Costanza-Robinson, M.S., Estabrook, B.D., and Fouhey, D.F.: Representative elementary volume estimation for porosity, moisture saturation, and air-water interfacial areas in unsaturated porous media: Data quality implication, Water Resour. Res., 47, W07513, 2011.

Erning, K., Grandel, S., Dahmke, A., and Schäfe, D.: Simulation of DNAPL infiltration and spreading behavior in the saturated zone at varying flow velocities and alternating subsurface geometries, Environ. Earth Sci., 65, 1119-1131, 2012.

Esfandiar, A., Radha, B., Wang, F.C., Yang, Q., Hu, S., Garaj, S., Nair, R.R., Geim, A.K., and Gopinadhan, K.: Size effect in ion transport through angstrom-scale slits, Science, 358, 511-513, 2017.

Fernandes, J.S., Appoloni, C.R., and Fernandes, C.P.: Determination of the Representative Elementary Volume for the study of sandstones and siltstones by X-Ray microtomography, Mater. Res., 15(4), 662-670, 2012.

Ghilardi, P., Kai, A.K., and Menduni, G.: Self-similar heterogeneity in granular porous media at the representative elementary volume scale, Water Resour. Res., 29(4), 1205-1214, 1993.

Gilevska, T., Passeport, E., Shayan, M., Seger, E., Lutz, E.J., West, K.A., Morgan, S.A., Mack, E.E., and Lollar, B.S.: Determination of in situ biodegradation rates via a novel high resolution isotopic approach in contaminated sediments, Water Res, 149,

632-639, 2019.

Hendrick, A.G., Erdmann, R.G., and Goodman, M.R.: Practical Considerations for Selection of Representative Elementary Volumes for Fluid Permeability in Fibrous Porous Media, Transp. Porous Med., 95, 389-405, 2012.

Kang, Q.J., Zhang, D.X., and Chen, S.Y.: Simulation of dissolution and precipitation in porous media, J. Geophys. Res. 108, NO. B10, 2505, doi:10.1029/2003JB002504, 2003.

Kim, J., and Mohanty, B.P.: Influence of lateral subsurface flow and connectivity on soil water storage in land surface modeling, J. Geophys. Res. Atmos., 121,704-721, 2016.

Lei, S., and Shi, Y.: Separate-phase model and its lattice Boltzmann algorithm for liquid-vapor two-phase flows in porous media, Phys. Rev. E, 99, 053302, 2019.

Martínez, F.S.J., Caniego, F.J., García-Gutiérrez, C., and Espejo, R.: Representative elementary area for multifractal analysis of soil porosity using entropy dimension, Nonlin. Processes Geophys., 14, 503-511, 2007.

Müller, C., and Siegesmund, S.: Evaluation of the representative elementary volume (REV) of a fractured geothermal sandstone reservoir, Environ. Earth Sci., 61, 1713-1724, 2010.

Niemet, M.R., and Selker, J.S.: A new method for quantification of liquid saturation in 2D translucent porous media systems using light transmission, Adv. Water Resour., 24, 651-666, 2001.

Nordahl, K., and Ringrose, P.S.: Identifying the Representative Elementary Volume for

553 permeability in heterolithic deposits using numerical rock models, Math Geosci.,
554 40, 753-771, 2008.
555 O'Carroll, D.M., Bradford, S.A., and Abriola, L.M.: Infiltration of PCE in a system
556 containing spatial wettability variations, J. Contam. Hydrol., 73, 39-63, 2004.
557 Pereira Nunes, J.P., Blunt, M.J., and Bijeljic, B.: Pore-scale simulation of carbonate
558 dissolution in micro-CT images, J. Geophys. Res. Solid Earth, 121, 558-576, 2016.
559 Piccoli, I, Schjønning, P., Lamandé, M., Zanini, F., and Morari, F.: Coupling gas transport
560 measurements and X-ray tomography scans for multiscale analysis in silty soils,
561 Geoderma, 338, 576-584, 2019.
562 Razavi, M.R., Muhunthan, B., and Al Hattamleh, O.: Representative elementary volume
563 analysis of sands using x-ray computed tomography, Geotech. Test J., 30(3), 212-
564 219, 2007.
565 Rozenbaum, O., and du Roscoat, S.R.: Representative elementary volume assessment of
566 three-dimensional x-ray microtomography images of heterogeneous
567 materials:Application to limestones, Phys. Rev. E, 89, 053304, 2014.
568 Teruel, F.E., and Rizwan-uddin: Numerical computation of macroscopic turbulence
569 quantities in representative elementary volumes of the porous medium, Int. J. Heat
570 Mass Transfer., 53, 5190-5198, 2010.
571 Ukrainczyk, N., and Koenders, E.A.B.: Representative elementary volumes for 3D
572 modeling of mass transport in cementitious materials, Modelling Simul. Mater. Sci.
573 Eng., 22, 035001, 2014.
574 Wang, L., Mi, J., and Guo, Z.: A modified lattice Bhatnagar–Gross–Krook model for

575 convection heat transfer in porous media, Int. J. Heat Mass Transfer., 94, 269-291,
576 2016.
577 Wang, S., Elsworth, D., and Liu, J.: A mechanistic model for permeability evolution in
578 fractured sorbing media, J. Geophys. Res, 117, B06205,
579 doi:10.1029/2011JB008855, 2012.
580 Wu, M., Wu, J.F., and Wu, J.C.: Simulation of DNAPL migration in heterogeneous
581 translucent porous media based on estimation of representative elementary volume,
582 J. Hydrol., 553, 276-288, 2017.
583 Wu, M., Wu, J.F., Wu, J.C., and Hu, B.X.: Effects of microarrangement of solid particles on
584 PCE migration and its remediation in porous media, Hydrol. Earth Syst. Sci., 22,
585 1001-1015, 2018.
586

587 **Table 1.** Experimental conditions

Experiment	I	II	III
Sandbox dimensions (cm)	20×15	60×45	60×45
Background translucent silica sand	F40/50	F20/30	F20/30
Medium condition	Homogeneity	Homogeneity	Heterogeneity
Median grain diameter (mm)	0.36	0.72	0.72
Permeability (m^2)	4.25×10^{-11}	1.35×10^{-10}	1.35×10^{-10}
V_{PCE} (ml)	9	32	40
Injection rate (ml/min)	0.5	0.5	0.5

588

589

590 **Table 2.** The fitted equations of frequency for REVs of porosity, density and tortuosity

Experiment		I	II	III
θ-REV	ω	-2.11×10^{-4}	-1.45×10^{-3}	7.63×10^{-4}
	ϵ	1.73	3.45	3.18
	ν	4.35	7.90	6.50
	R^2	0.938	0.924	0.907
ρ-REV	ω	-6.51×10^{-4}	-2.51×10^{-4}	1.51×10^{-3}
	ϵ	1.08	1.66	2.40
	ν	2.89	2.97	3.70
	R^2	0.967	0.990	0.859
τ-REV	ω	-3.36×10^{-4}	-2.04×10^{-4}	1.29×10^{-3}
	ϵ	1.39	2.15	1.20
	ν	3.65	4.20	1.05
	R^2	0.769	0.875	0.919

591 *θ represents porosity, ρ represents density, τ represents tortuosity; ω, ϵ and ν are fitted parameters
592 of the model
593
594

Table 3. The fitted equations between average value of REV and d_I, d_m

	Experiment	d_m	d_I
I	S_o-REV	$\overline{REV} = -1.67 \times 10^{-3} d_m^2 + 0.193 d_m + 2.72$ (R^2=0.807)	$\overline{REV} = -1.97 \times 10^{-3} d_I^2 + 0.245 d_I + 1.12$ (R^2=0.832)
	A_{OW}-REV	$\overline{REV} = -6.10 \times 10^{-4} d_m^2 + 5.82 \times 10^{-2} d_m + 7.20$ (R^2=0.401)	$\overline{REV} = -1.47 \times 10^{-3} d_I^2 + 0.205 d_I + 1.84$ (R^2=0.733)
II	S_o-REV	$\overline{REV} = -4.08 \times 10^{-5} d_m^2 + 1.50 \times 10^{-2} d_m + 7.54$ (R^2=0.655)	$\overline{REV} = -3.94 \times 10^{-5} d_I^2 + 7.80 \times 10^{-3} d_I + 8.50$ (R^2=0.327)
	A_{OW}-REV	$\overline{REV} = -1.92 \times 10^{-5} d_m^2 + 4.47 \times 10^{-3} d_m + 9.46$ (R^2=0.616)	$\overline{REV} = -1.92 \times 10^{-5} d_I^2 + 4.47 \times 10^{-3} d_I + 9.46$ (R^2=0.616)
III	S_o-REV	$\overline{REV} = -6.06 \times 10^{-6} d_m^2 + 2.27 \times 10^{-3} d_m + 7.76$ (R^2=0.153)	$\overline{REV} = 1.69 \times 10^{-5} d_I^2 - 1.21 \times 10^{-2} d_I + 9.62$ (R^2=0.236)
	A_{OW}-REV	$\overline{REV} = -8.71 \times 10^{-6} d_m^2 + 5.66 \times 10^{-3} d_m + 11.5$ (R^2=0.115)	$\overline{REV} = -1.50 \times 10^{-5} d_I^2 + 7.88 \times 10^{-3} d_I + 11.4$ (R^2=0.150)

*$\overline{REV}$ is the average value of REV size, d_m is the distance from mass center of PCE plume to the cell contained in PCE plume, d_I is the distance from injection point to the cell contained in PCE plume

601 **Table 4.** The fitted relationship between REV and S_o

Experiment	S_o-REV	A_{OW}-REV
I	$\mathrm{REV} = -2.13 \times \ln S_o + 0.876$ (R^2=0.466)	$\mathrm{REV} = 2.27e^{2.70 \times S_o}$ (R^2=0.366)
II	$\mathrm{REV} = -0.961 \times \ln S_o + 1.09$ (R^2=0.415)	$\mathrm{REV} = 1.70e^{3.30 \times S_o}$ (R^2=0.500)
III	$\mathrm{REV} = -1.40 \times \ln S_o + 3.96$ (R^2=0.538)	$\mathrm{REV} = 2.05e^{3.22 \times S_o}$ (R^2=0.573)

602

603

Figure Captions

Figure 1. (a) Variable changes as measured scale (L) increment in conceptual curve (Costanza-Robinson et al., 2011); (b) Scale effect and the cuboid image window geometry; (c) System Device for acquisition of parameters (porosity and density, etc.) of translucent material; (d) The infinitesimal selected from translucent porous media packed in 2D sandbox.

Figure 2. (a) The system sandbox equipment of Experiment-I; (b) The system sandbox equipment of Experiment-II; (c) The system sandbox equipment of Experiment-III

Figure 3. (a) The emergent light intensity, porosity, permeability and tortuosity of 2D translucent silica sand for Experiments-I-III; (b) The PCE saturation of Experiments-I-III during 0~1523 min and observation cells

Figure 4. (a) The change of porosity (θ), associated coefficient of variation (C_V^i), entropy dimension (DI^i), the relative gradient error (ε_g^i), and new criterion-χ^i for observation cells as cuboid window scale (L) increases; (b) The change of PCE saturation (S_o), associated C_V^i, DI^i, ε_g^i, and χ^i for observation cells as cuboid window scale (L) increases

Figure 5. (a) The distributions of minimum REV sizes of porosity, sand density and tortuosity for Experiments-I-III; (b) The frequency of minimum REV sizes of Experiments and fitted models

Figure 6. (a) The distributions of S_o-REV sizes during 0~1523 min for Experiments-I-III; (b) The distributions of A_{OW}-REV sizes during 0~1523 min for Experiments-I-III

Figure 7. (a) The mass center coordinate of PCE plume, GTP, plume area and the mean, standard deviation of S_o-REV and A_{OW}-REV during 0~1523 min; (b) The change of

627 average REV size as the distance d_I, d_m increases and fitted relationship between

628 REV sizes and S_o for Experiments-I and II

629 **Fig. 1**

630

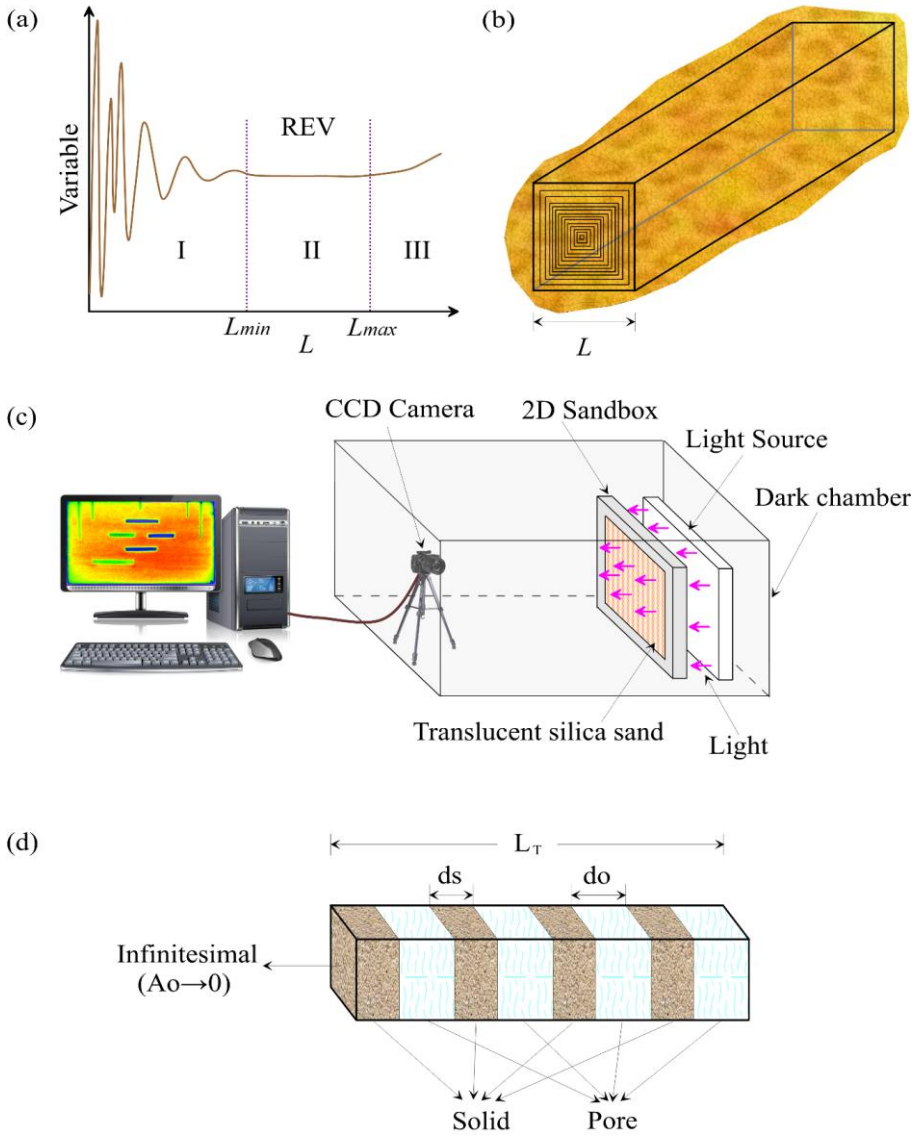

631

632

633 **Fig. 2**

634

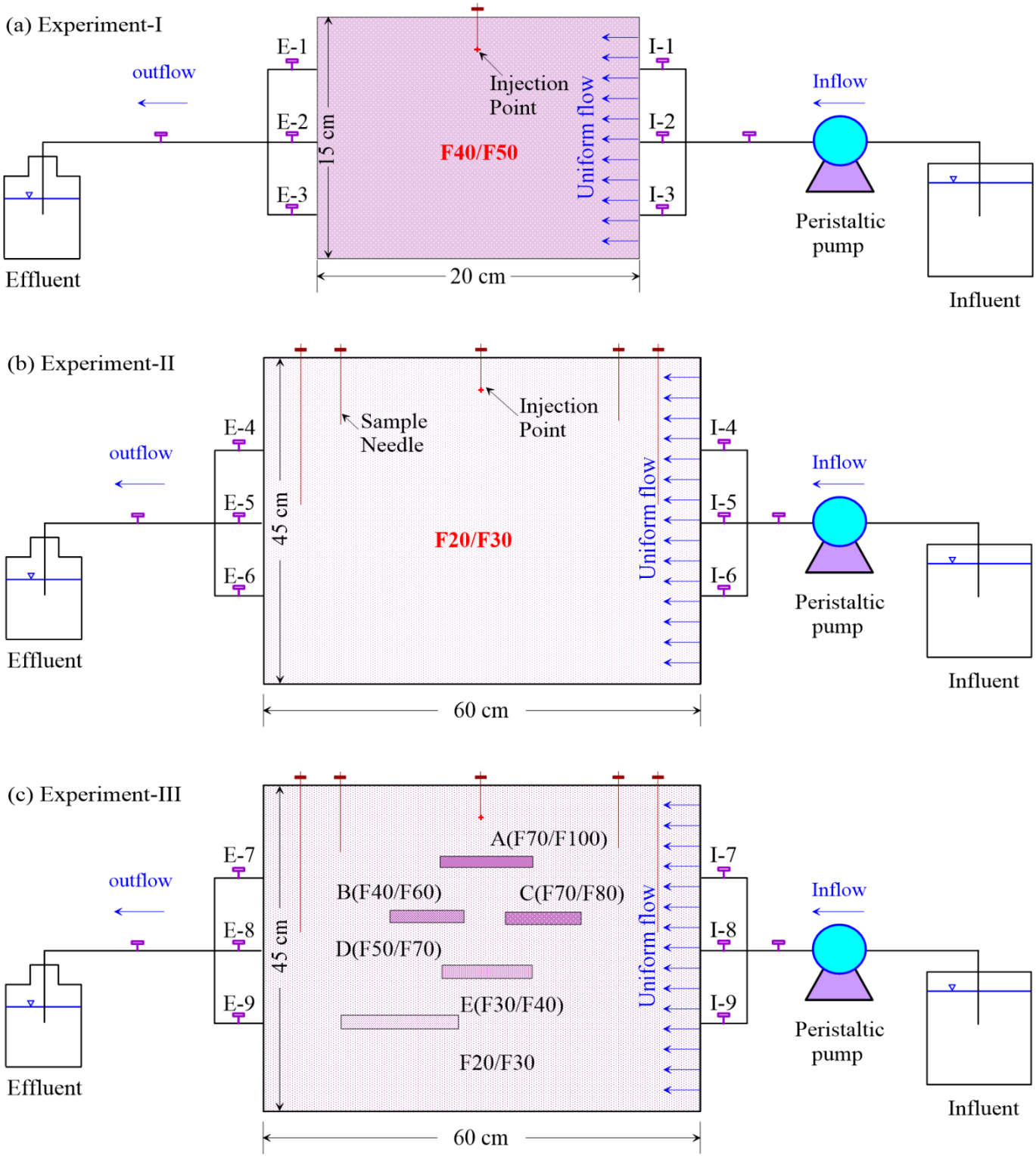

635

636

Fig. 3

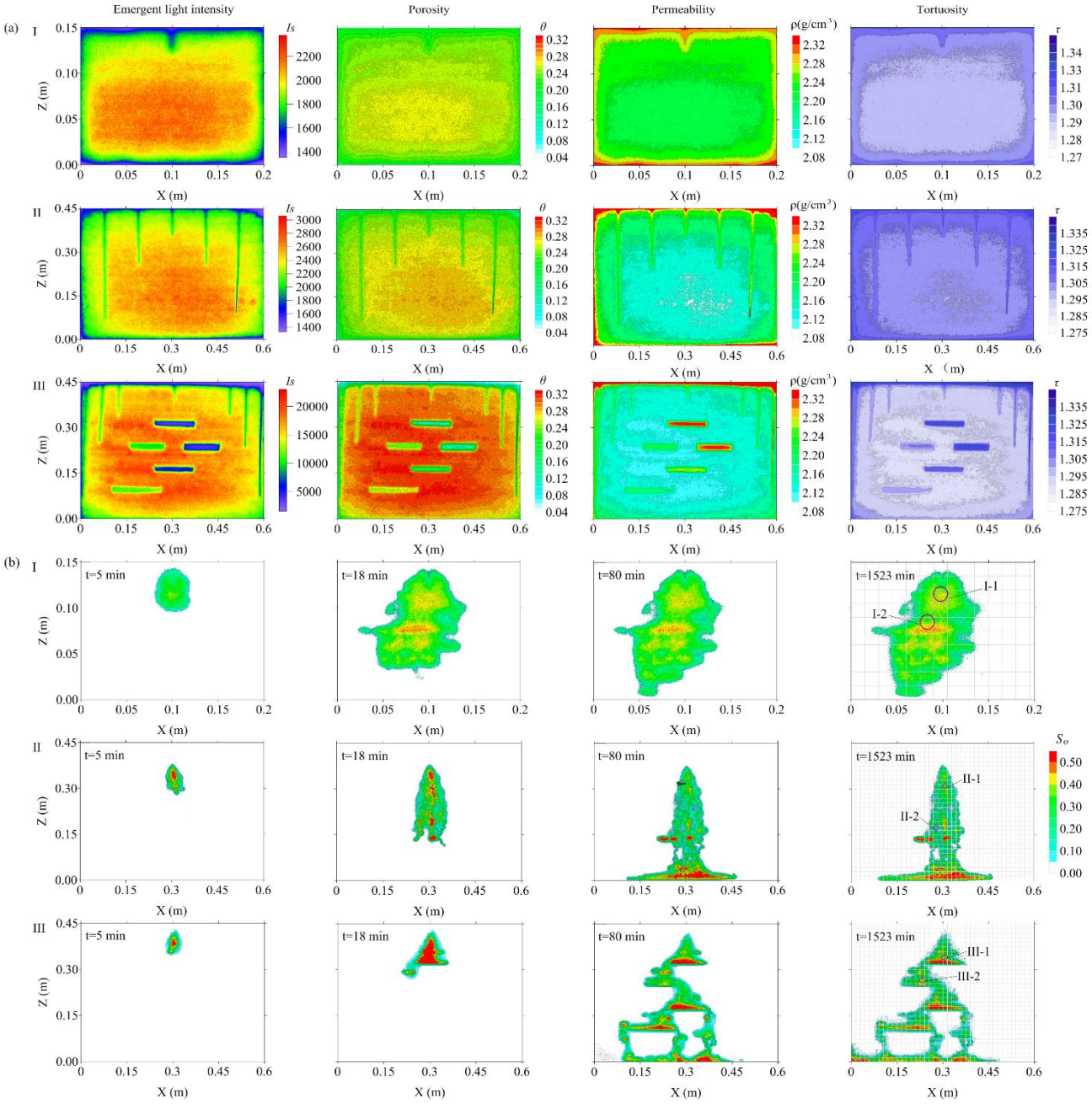
(a)
Emergent light intensity
Porosity
Permeability
Tortuosity
I
II
III
Z (m)
X (m)
Is
θ
ρ(g/cm³)
τ
(b)
t=5 min
t=18 min
t=80 min
t=1523 min
I-1
I-2
II-1
II-2
III-1
III-2
So

640 **Fig. 4**

641

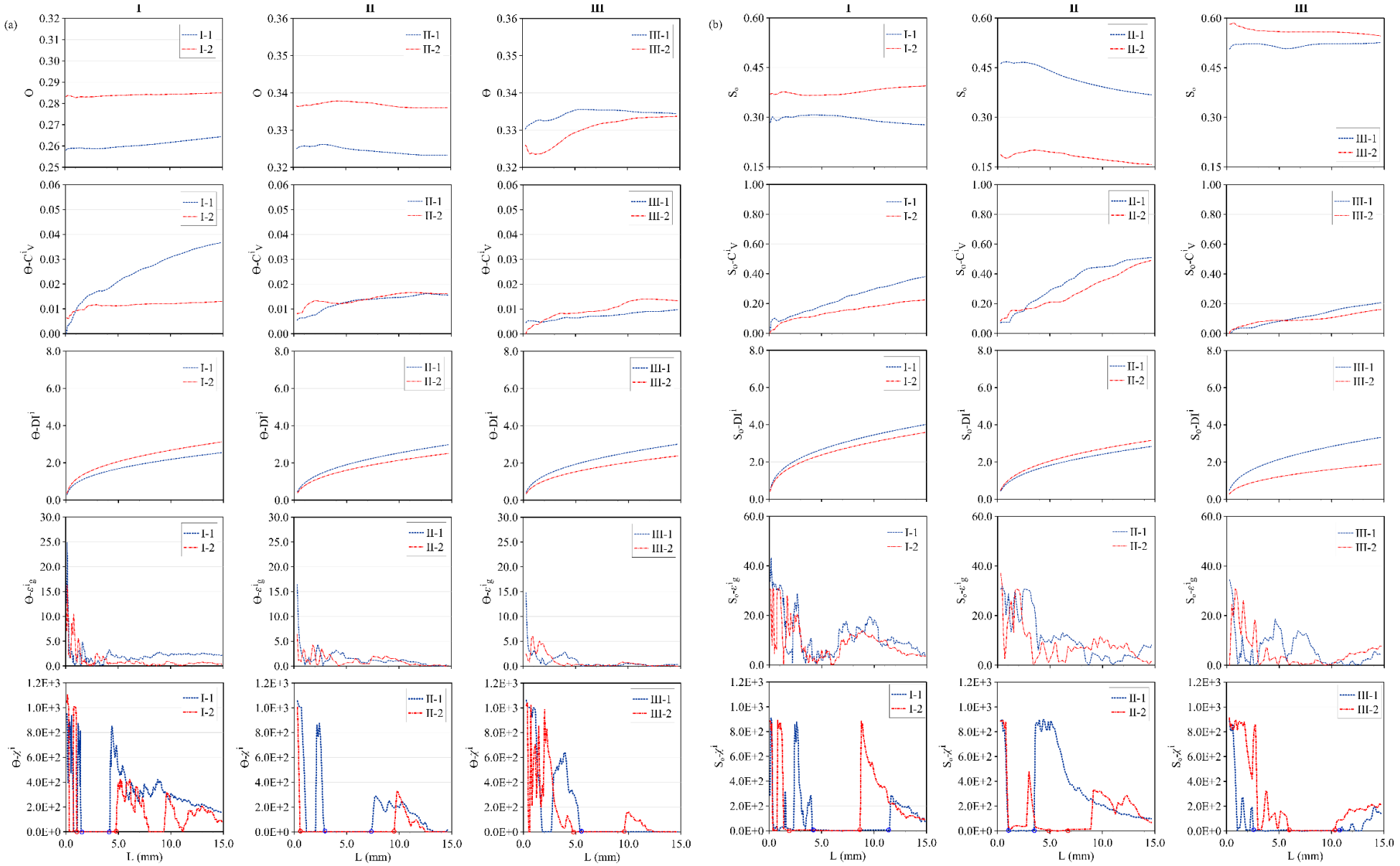

642

Fig. 5

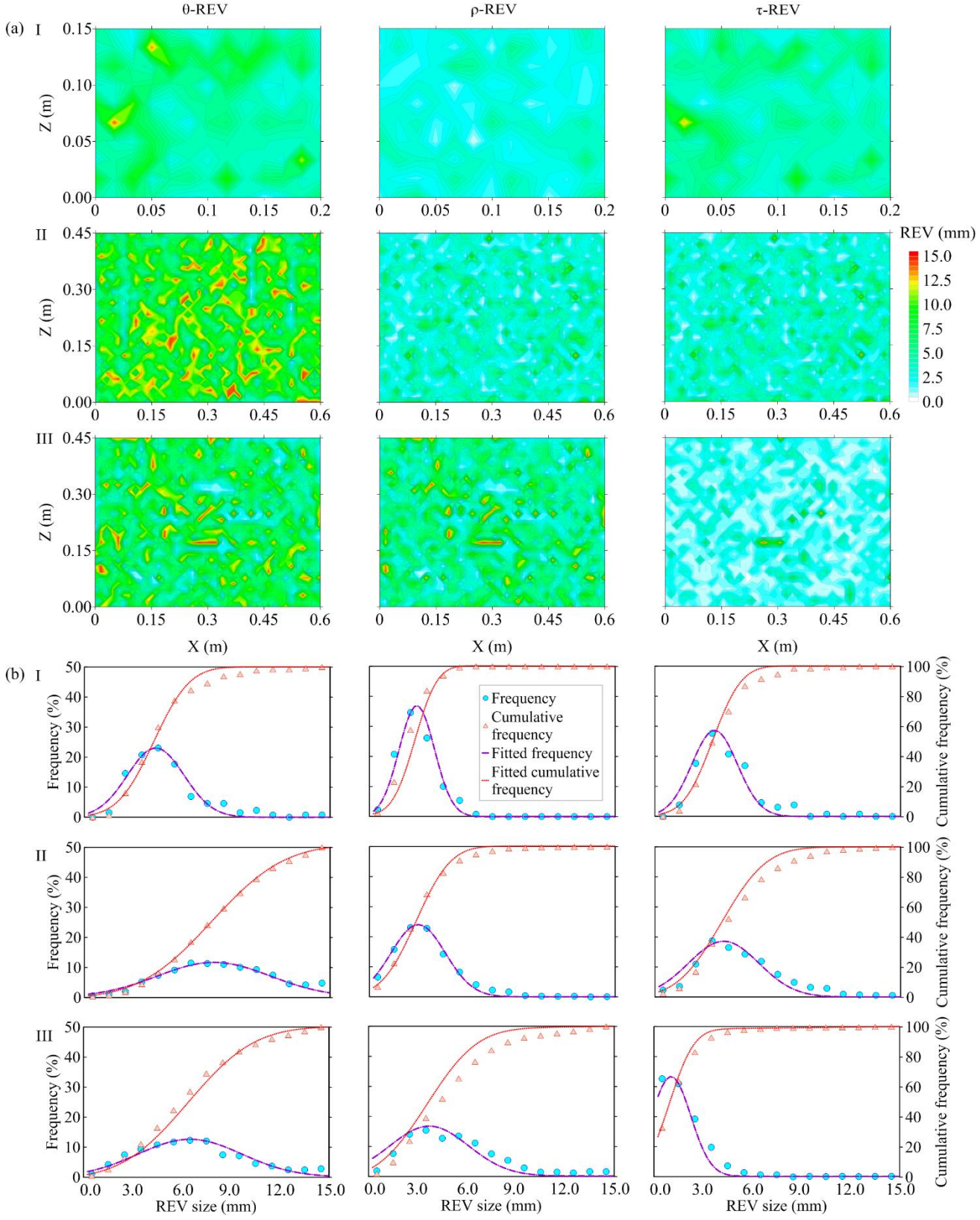
(a)
θ-REV
ρ-REV
τ-REV
I
II
III
Z (m)
REV (mm)
15.0
12.5
10.0
7.5
5.0
2.5
0.0
X (m)
(b)
Frequency (%)
Cumulative frequency (%)
Frequency
Cumulative frequency
Fitted frequency
Fitted cumulative frequency
REV size (mm)

Fig. 6

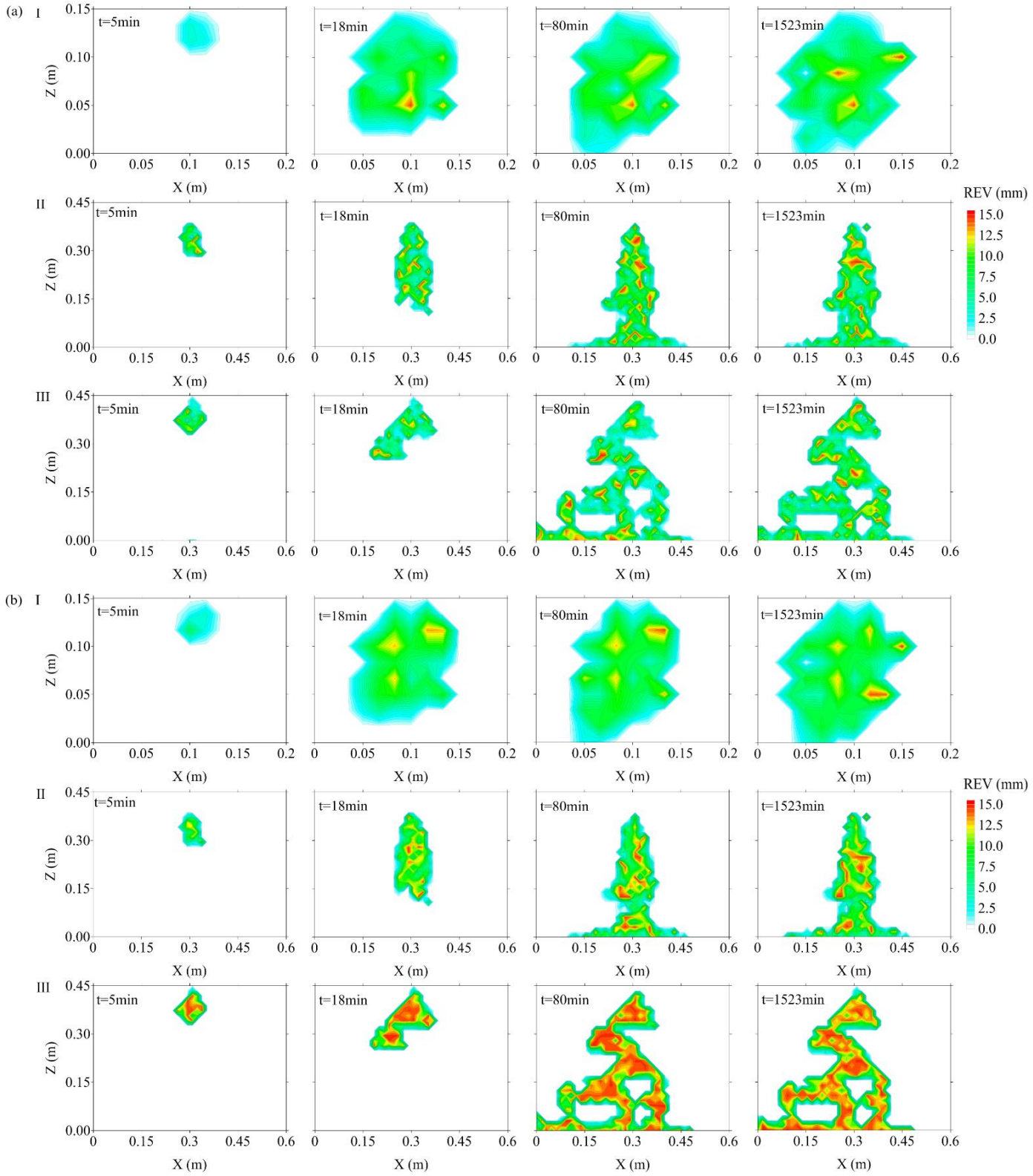
(a)
I
II
III
t=5min
t=18min
t=80min
t=1523min
Z (m)
X (m)
REV (mm)
15.0
12.5
10.0
7.5
5.0
2.5
0.0
(b)
I
II
III
t=5min
t=18min
t=80min
t=1523min
Z (m)
X (m)
REV (mm)
15.0
12.5
10.0
7.5
5.0
2.5
0.0

Fig. 7

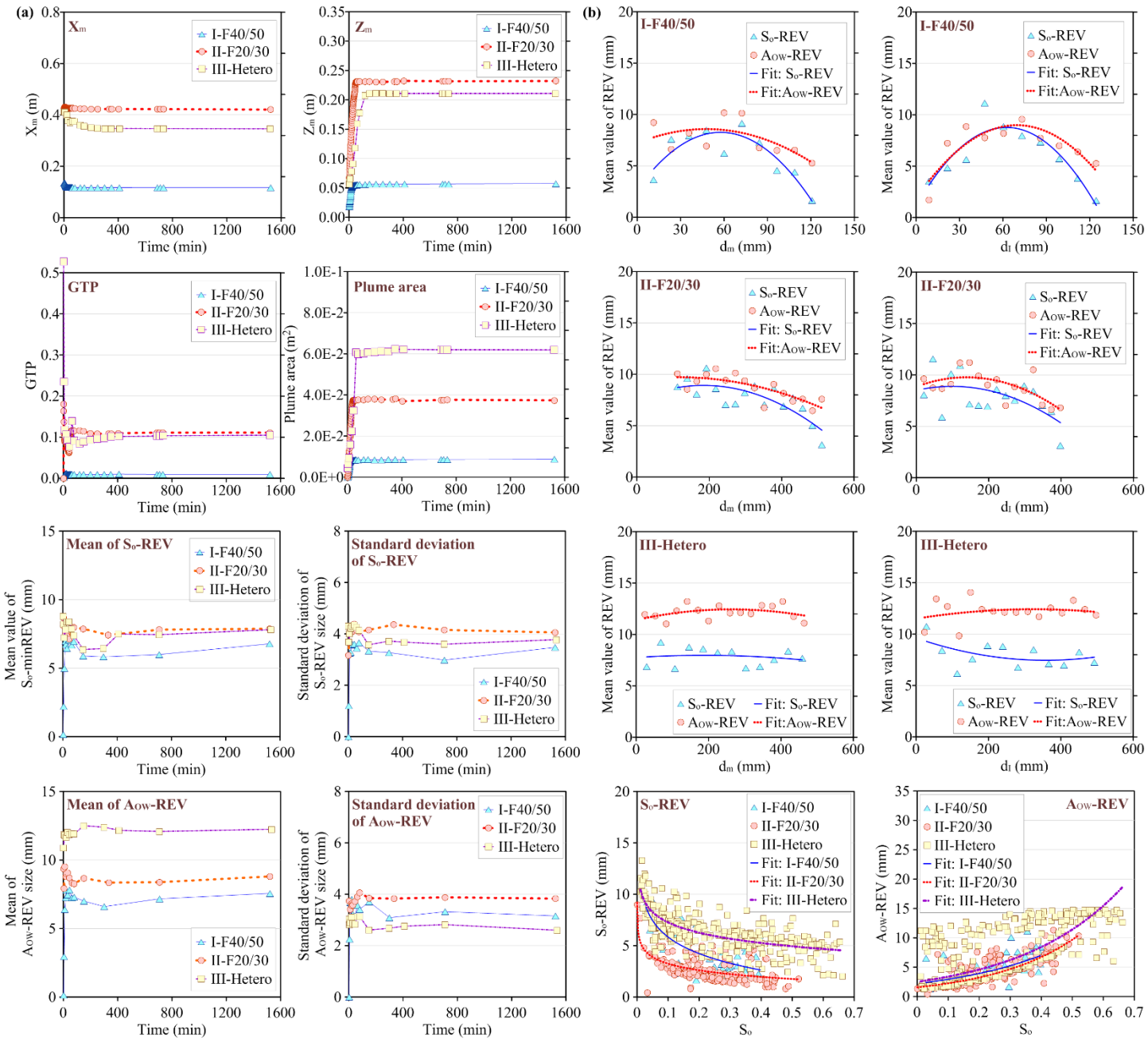
(a)
Xm
Zm
GTP
Plume area
Mean value of So-REV
Standard deviation of So-REV
Mean of Aow-REV
Standard deviation of Aow-REV
I-F40/50
II-F20/30
III-Hetero
Time (min)
(b)
So-REV
Aow-REV
Fit: So-REV
Fit:Aow-REV
Mean value of REV (mm)
dm (mm)
dI (mm)
Fit: I-F40/50
Fit: II-F20/30
Fit: III-Hetero
So